Active metal brazing of Al_2O_3 to Kovar® (Fe–29Ni–17Co wt.%) using Copper ABA® (Cu–3.0Si–2.3Ti–2.0Al wt.%)

Majed Ali[a], Kevin M. Knowles[a,*], Phillip M. Mallinson[b], John A. Fernie[b]

[a]*Department of Materials Science and Metallurgy, University of Cambridge, 27 Charles Babbage Road, Cambridge, CB3 0FS, UK*
[b]*AWE plc, Aldermaston, Reading, Berkshire, RG7 4PR, UK*

Abstract

The application of an active braze alloy (ABA) known as Copper ABA® (Cu–3.0Si–2.3Ti–2.0Al wt.%) to join Al_2O_3 to Kovar® (Fe–29Ni–17Co wt.%) has been investigated. This ABA was selected to increase the operating temperature of the joint beyond the capabilities of typically used ABAs such as Ag–Cu–Ti-based alloys.

Silica present as a secondary phase in the Al_2O_3 at a level of ~5 wt.% enabled the ceramic component to bond to the ABA chemically by forming a layer of Si_3Ti_5 at the ABA/Al_2O_3 interface. Appropriate brazing conditions to preserve a near-continuous Si_3Ti_5 layer on the Al_2O_3 and a continuous Fe_3Si layer on the Kovar® were found to be a brazing time of ≤15 min at 1025 °C or ≤2 min at 1050 °C. These conditions produced joints that did not break on handling and could be prepared easily for microscopy. Brazing for longer periods of time, up to 45 min, at these temperatures broke down the Si_3Ti_5 layer on the Al_2O_3, while brazing at ≥1075 °C for 2–45 min broke down the Fe_3Si layer on the Kovar® significantly. Further complications of brazing at ≥1075 °C included leakage of the ABA out of the joint and the formation of a new brittle silicide, $Ni_{16}Si_7Ti_6$, at the ABA/Al_2O_3 interface.

This investigation demonstrates that it is not straightforward to join Al_2O_3 to Kovar® using Copper ABA®, partly because the ranges of suitable values for the brazing temperature and time are quite limited. Other approaches to increase the operating temperature of the joint are discussed.

Keywords: Brazing, Joining, Alumina, Al_2O_3, Kovar, Copper ABA.

* Corresponding author.
E-mail address: kmk10@cam.ac.uk (K.M. Knowles).

1. Introduction

Among the current techniques to join ceramics to ceramics and to metals, a plethora of which have been reviewed in [1], active metal brazing is a relatively simple technique. This particular brazing method avoids a separate step of metallising the bonding surface of the ceramic to make it more wettable by a conventional braze alloy, such as the Ag–28Cu wt.% eutectic alloy. This is achieved by incorporating an element into the braze alloy which can react with the ceramic to form a phase over which the liquid braze can spread; the resultant braze alloy is referred to as an active braze alloy (ABA). The majority of studies on the active metal brazing of Al_2O_3 have used ABAs based on the Ag–Cu system with added Ti, typically at a level of about 1 to 5 wt.% Ti [2,3]. Other group IV and V elements such as Zr, Hf and V can also be added to Ag, Cu and Ag–Cu alloys [4,5,6,7], but the resultant binary and ternary ABAs have received far less attention than the Ag–Cu–Ti system.

An application has been identified in which Al_2O_3 is joined to a iron–nickel–cobalt alloy with the composition Fe–29Ni–17Co wt.%, also known as Kovar®. The brazing of Al_2O_3 and Kovar® using a commonly used commercially available Ag–Cu–Ti-based alloy known as Cusil ABA®, with the composition Ag–35.25Cu–1.75Ti wt.%, has been studied in some detail recently [8]. In terms of temperature capability Ag–Cu–Ti-based ABAs are not recommended for use above 600 °C because of creep and oxidation of the ABA [9]. In order to increase the maximum operating temperature of a composite containing a Al_2O_3–Kovar® bond, the use of a commercially available Cu-based ABA known as Copper ABA®, with the composition Cu–3.0Si–2.3Ti–2.0Al wt.%, has been investigated in this work. There are a number of other commercially available high temperature ABAs such as Gold ABA® (Au–3.0Ni–0.6Ti wt.%), Nioro®-ABA (Au–15.5Ni–0.75Mo–1.75V wt.%) and Gold-ABA-V® (Au–0.75Ni–1.75V wt.%). However, the high gold content in these ABAs makes them very expensive and more suited to specialist high temperature applications.

Copper ABA® melts between 958 and 1024 °C, and so a relatively high brazing temperature is required to produce a bond with this braze alloy. This braze alloy is more ductile than Cusil ABA®, which may help to accommodate thermally-induced stresses that develop in a joint; elongations for sheets of Copper ABA® and Cusil

ABA® with equivalent dimensions are reported as 42% and 20%, respectively [10]. Literature on the brazing of various ceramics using Copper ABA® is available, such as Si_3Ni_4 brazed to itself with and without various metallic spacers [11–13], Y_2O_3-stabilised-ZrO_2 brazed to a stainless steel [14] and SiC-fibre-bonded-ceramics (SA-Tyrannohex™) brazed to themselves [15]. No literature on the brazing of Al_2O_3 using this alloy has been found. There are a number of experimental Cu-based ABAs with additions of Ga and Sn, along with Ti, V or Zr as active element wetting agents [16–18]. The work of Lin et al. [18] shows that Cu–Sn–Ti-based alloys have the potential to spread on Al_2O_3 and chemically bond to Al_2O_3. In their work, the ability to wet Al_2O_3 using a range of Cu–Sn–Ti-based alloys containing 6–12 wt.% Ti and 21 wt.% Sn was investigated. An addition of 9 wt.% Ti demonstrated the best wetting ability, with contact angles being consistently lower compared to other alloy compositions over a period of 30 min at 900 °C and approaching zero after 25 min.

The objectives of this work have been to determine whether Copper ABA® can be used to bond Al_2O_3 to Kovar® chemically and, if so, to determine suitable values for various brazing parameters, such as the peak temperature (T_p) and time at T_p (τ). 99.7 and 95 wt.% Al_2O_3 have been used to study the extent to which silica-based secondary phases in the Al_2O_3 participate in the chemical reactions at the ABA/Al_2O_3 interface. Joints were brazed at a T_p between 1025 and 1100 °C for 0–45 min.

2. Experimental

2.1. Materials

Copper ABA® (Cu–6.3Si–2.8Ti–4.4Al at.%), which melts between 958 and 1024 °C, has been used to join Kovar® to 95 and 99.7 wt.% Al_2O_3. The ABA was supplied by VBC Group Ltd (UK) in foil form, with a thickness of ~65 μm, from which 10 × 5 mm sections were taken for joining. An investigation of the as-received ABA using a scanning electron microscope (SEM) showed that it contained CuSiTi, with a composition measured by energy dispersive X-ray spectroscopy (EDS) of 33Cu–33Si–34Ti at.%, randomly distributed in a solid solution of Si and Al in Cu (92Cu–4Si–4Al at.%), as shown in the back-scattered electron images (BSEIs) given in Figure 1. Si_3Ti_5

particles, with a composition of 37Si–61Ti–2Cu at.%, were also found within some of the CuSiTi particles.

Braze joints made with 95 wt.% Al_2O_3 were compared with joints made with high purity 99.7 wt.% Al_2O_3. Manufacturer's data gave the densities of the two ceramics as 3.7 Mg m^{-3} and > 3.9 Mg m^{-3} respectively, with grain sizes of 3–8 and 3–10 μm respectively. Calculated levels of porosity in the two ceramics were 7% and < 2% respectively. Electron microprobe analysis of the bonding surfaces of both Al_2O_3 ceramics was performed to determine their composition. A Cameca SX-100 (France) electron microprobe operated at 15 kV with a 10 nA electron beam was used in the wavelength-dispersive mode. Calibration of the elements of interest used several mineral standards. The compositions of the ceramics are given in Table 1. The Si in the 95 wt.% Al_2O_3 was in the form of intergranular amorphous silica and the Zr was in the form of zirconia particles approximately 4 μm in diameter randomly distributed throughout the ceramic. The zirconia might have been incorporated into the Al_2O_3 during a milling process that employed zirconia grinding media to produce fine Al_2O_3 powder prior to sintering. Al_2O_3 in the form of 10 × 5 × 4 mm plates were brazed to 10 × 5 × 0.5 mm plates of Kovar®. Prior to brazing, all of the components of the joints were cleaned separately in an ultrasonic bath of detergent for up to 15 min.

The as-received Kovar® was composed of equiaxed grains of various sizes, ranging from ~10 to ~100 μm in width, all of which had a face-centered cubic close packed crystal structure with a lattice parameter of a = 3.6 Å measured by X-ray diffraction. Its composition was measured by EDS as Fe–28Ni–17Co at.%.

2.2. Brazing process

Al_2O_3/Copper ABA®/Kovar® joints were prepared in an atmosphere of purified argon, which was established in a horizontal electric furnace (STF 15/450, Carbolite, UK) as described in [3]. Air Products and Chemicals (USA) BIP® technology was used to purify the argon gas entering the furnace. A heating rate of 10 °C min^{-1} was used. The cooling rate was ~15 °C min^{-1} between the peak temperature used and ~500 °C, after which it reduced significantly during a furnace cool to room temperature. A pressure of ~4 kPa was applied to all of the joints using a 20 g weight to improve contact across the components.

The combinations of T_p and τ used to braze the two types of Al_2O_3 are given in Table 2. Brazing of 95 wt.% Al_2O_3 was carried out with T_p ranging from the liquidus temperature of the ABA of 1025 °C up to 1100 °C. For these brazing experiments τ varied between 0 and 45 min. The low quantity of secondary phase in 99.7 wt.% Al_2O_3 made it difficult to establish a bond between the Al_2O_3 and the ABA. Consequently, less work was undertaken on the brazing of this ceramic, with τ ranging from 0 to 45 min at a T_p of 1025 °C, as described in Table 2.

2.3. Analytical processes

A field emission SEM, Leo 1530 VP, Leo Electron Microscopy - Carl Zeiss®, Germany, operated at 20 kV was used to observe the microstructures of joints, before undertaking more detailed examinations of joints by transmission electron microscopy. This microscope was equipped with an energy dispersive spectrometer (INCA-7426, Oxford Instruments®, UK). At least four cross-sections of each joint were analysed with this microscope to monitor the homogeneity of the interfacial structures and the chemistry across the joint. A low speed diamond saw was used to cut out cross-sections of joints, which were then mounted in acrylic resin at room temperature, polished and coated with a thin layer of carbon before observations were made. It was necessary to mount all joints made with 99.7 wt.% Al_2O_3 and the joints made with 95 wt.% Al_2O_3 using a $T_p \geq 1075$ °C or 1050 °C with $\tau \geq 15$ min in clear resin before cutting out cross-sections. This is because the Al_2O_3 typically separated from the ABA while cutting.

A scanning transmission electron microscope (STEM), Tecnai Osiris™, FEI, USA, operated at 200 kV was also used to perform elemental analysis using an EDS system (Super-X system, FEI, USA). Thin sections of joints were prepared for STEM analysis using a focused ion beam instrument, FIB, (Helios Nanolab™, FEI, USA). The procedure commonly known as the lift-out technique [19] was used to transfer sections of joints up to 25 × 10 μm to molybdenum grids, or a carbon substrate on a molybdenum grid. These sections were subsequently reduced to a thickness of ~100 nm using the FIB.

Selected area diffraction patterns were collected to determine the crystal structures of phases using a conventional transmission electron microscope (TEM), 200CX,

JEOL®, Japan, which was operated at 200 kV. The camera length of this microscope was monitored at regular intervals using an Al thin film, which was supplied by Agar Scientific, UK.

The thicknesses of the reaction layers were measured as a function of T_p and τ from images collected using the SEM; a mean value and ± one standard deviation from twenty five measurements are reported.

3. Results

3.1. Brazing 95 wt.% Al_2O_3 to Kovar®

The microstructure of the joints made with 95 wt.% Al_2O_3 was strongly affected by the T_p used, particularly the state of the ABA/Al_2O_3 interface. Therefore, the microstructures produced at each T_p used are discussed separately and as a function of τ.

3.1.1. Brazing 95 wt.% Al_2O_3 at 1025 °C

BSEIs of cross-sections of 95 wt.% Al_2O_3–Kovar® joints that were held at 1025 °C for 0 to 45 min are shown in Figure 2. Brazing at this temperature for a nominal 1 s before cooling was sufficient to melt the ABA completely and to bond chemically the ABA to both the Al_2O_3 and Kovar®. Typically, one phase was observed at the ABA/Al_2O_3 interface in the form of a 1.7 μm thick broken layer with a composition of 37Si–61Ti–2Cu at.%. The crystal structure of the particles in this layer was identified by electron diffraction as that of Si_3Ti_5 (hexagonal, $P6_3/mcm$, space group 193) with the lattice parameters a = 7.8 Å and c = 5.4 Å; a selection of indexed electron diffraction patterns is shown in Figure 3. The silica in the Al_2O_3 appears to react with the Ti in the ABA to form Si_3Ti_5, which consequently bonds the Al_2O_3 component chemically to the ABA. Although there is silicon in the molten braze, evidence such as that in Figure 2 shows clearly that Si_3Ti_5 is only found at the interface with Al_2O_3 – it is not found within the braze away from the Al_2O_3 interface. Hence, while the silicon in the braze is able to participate in the formation of Si_3Ti_5, the clear evidence is that the interface with the alumina acts as a favourable nucleation site for Si_3Ti_5, because otherwise Si_3Ti_5 would be seen elsewhere in the joint, rather than just at the interface with Al_2O_3.

Particles with a composition of 22Cu–7Ni–3Fe–1Co–34Si–33Ti at.% were occasionally observed between the Si_3Ti_5 layer and the ABA, specifically at regions where the ABA was directly in contact with a large quantity of silica in the Al_2O_3, as shown in Figure 4. The crystal structure of these particles was identified by electron diffraction as that of CuSiTi (orthorhombic, *Pnma*, space group 62) with the lattice parameters a = 6.4 Å, b = 3.9 Å and c = 7.4 Å; a selection of indexed electron diffraction patterns is shown in Figure 5. It is apparent that the Cu in the CuSiTi is partially substituted by the chemical elements of the Kovar®, particularly Ni and Fe.

In the same joint, four layers were observed near the Kovar® at all bonding times. One of these layers is in contact with the Kovar®, while the other three layers are separated from this layer by ~2 μm and are in the ABA. The layer on the Kovar® is comprised of large particles which extend across the entire width of the layer, ~ 4.5 μm, and are greater than 10 μm in length parallel to the Kovar®. Their composition was measured by EDS typically as 57Fe–15Si–12Ni–9Co–4Al–3Cu at.%. This measurement did not vary significantly normal to the Kovar®. The crystal structure of these particles was identified by electron diffraction as that of Fe_3Si (cubic, $Fm\bar{3}m$, space group 225) with the lattice parameter a = 5.9 Å; a selection of indexed electron diffraction patterns is shown in Figure 6. The EDS data suggests that these Fe_3Si particles can accommodate various elements in a solid solution, particularly Ni and Co. According to the Fe–Ni–Si phase diagram [20], Fe_3Si can accommodate significant amounts of Ni at ~T_p, approximately 26 at.% Ni at 1100 °C.

Furthermore, at all bonding times, a layer up to ~2 μm thick with a composition of 23Ni–14Fe–14Co–6Cu–23Si–20Ti at.% is separated from the Fe_3Si layer by a distance of ~2 μm. It appears that this layer formed on the Fe_3Si layer and subsequently broke away into the ABA, because there are some particles with the same composition on the Fe_3Si layer. A selection of electron diffraction patterns from the particles in this layer is shown in Figure 7. These patterns are consistent with the crystal structure of $Ni_{16}Si_7Ti_6$ (cubic, $Fm\bar{3}m$, space group 225) with the lattice parameter a = 11.8 Å. The composition of this layer is also consistent with $Ni_{16}Si_7Ti_6$ if it assumed that some of the Ni is substituted by elements of a similar size such as Fe, Co and Cu, and so this phase is referred to as $Ni_{16}Si_7Ti_6$.

There is a thin layer adjacent to the $Ni_{16}Si_7Ti_6$ layer that varies in thickness between ~50 and ~600 nm. The composition of this layer was measured by EDS in the STEM as 32Fe–29Ti–17Si–11Ni–9Co–2Cu at.%. The particles in this layer have the same crystal structure as Fe_2Ti (hexagonal, $P6_3/mmc$, space group 194) with the lattice parameters a = 5.2 Å and c = 8.8 Å. A selection of indexed electron diffraction patterns from these particles is shown in Figure 8. The EDS data suggests the Fe in Fe_2Ti is substituted by several elements, particularly Si. The maximum solubility of Si in Fe_2Ti is estimated at ~26 at.% Si between 800 and 1150 °C [21].

At all bonding times, there is another layer with the composition 14Cu–10Fe–9Ni–2Co–33Si–32Ti at.% adjacent to the Fe_2Ti layer. This layer is comprised of particles which have the same crystal structure as CuSiTi (orthorhombic, *Pnma*, space group 62) with the lattice parameters a = 6.4 Å, b = 4.0 Å and c = 7.3 Å; a selection of indexed electron diffraction patterns is shown in Figure 9. Some of the particles in this layer have broken away into the ABA, and so appear as individual CuSiTi particles alongside the CuSiTi layer. The extent of the substitution of Cu by Ni and Fe is much higher in these CuSiTi particles compared with the CuSiTi observed at the ABA/Al_2O_3 interface.

Increasing τ to 2 min produced larger Si_3Ti_5 particles on the Al_2O_3, but collectively they still formed a broken layer up to ~2.5 μm wide. The Al_2O_3 surface was almost completely covered by a layer of Si_3Ti_5 between 2 and 3 μm thick after brazing for 15 min. The columnar-like shape of some of the Si_3Ti_5 particles resulted in a large variation in the thickness of this layer. Increasing τ to 30 min caused the Si_3Ti_5 layer to break down, reducing its average thickness to 1.8 μm. Significant breakdown of the Si_3Ti_5 layer occurred after brazing for 45 min, resulting in the Si_3Ti_5 particles to separate from each other and also the Al_2O_3.

The thickness of the Fe_3Si layer on the Kovar® increases parabolically with time for joints brazed for 2–45 min at a T_p of 1025 °C, as shown graphically in Figure 10. Additional joints were brazed for 2 min between 1025 and 1100 °C to estimate the activation energy for growth of this layer. However, this was not possible because of two reasons. Firstly, some of the ABA flowed out of a number of joints prepared at 1075 and 1100 °C, which included those brazed for 2 min at these temperatures.

Secondly, the Fe_3Si layer breaks up slightly at a T_p between 1075–1100 °C to leave small Fe_3Si particles in the ABA between the Fe_3Si layer and the $Ni_{16}Si_7Ti_6$ layer. As a consequence, the mean thickness of this layer appears to decrease as T_p increases.

At a T_p between 1050 and 1075 °C, the mean thickness of the Fe_3Si layer initially increases as a function of τ, and then it reaches a maximum value before reducing. The reduction in the mean thicknesses is mainly caused by the breakdown of the Fe_3Si layer, which is amplified by increasing T_p. No significant changes in the composition of the Fe_3Si layer as a function of T_p and τ were identified, and so this breakdown process does not appear to be a consequence of any change in the composition of this layer.

The layered structure of $Ni_{16}Si_7Ti_6$, Fe_2Ti and CuSiTi near the ABA/Kovar® interface was continuous only in the joint heated to 1025 °C for 2 min. These phases were typically observed in the form of a broken layered structure or a collection of individual particles in joints prepared at higher T_p or by using longer τ. The Fe_2Ti phase was not always observed in all of the joints brazed at 1025 °C. Instead $Ni_{16}Si_7Ti_6$ was observed alongside CuSiTi. In other cases, the Fe_2Ti is difficult to identify from the BSEIs taken because it has a similar average atomic number compared to $Ni_{16}Si_7Ti_6$ and it is present in small amounts between the $Ni_{16}Si_7Ti_6$ and CuSiTi. Small fluctuations in the compositions of $Ni_{16}Si_7Ti_6$ and Fe_2Ti as a function of T_p and τ were measured, but no conclusive trends were identified. The variations in these compositions could be a result of $Ni_{16}Si_7Ti_6$ and Fe_2Ti having a small homogeneity range at temperatures close to the T_p used. EDS measurements indicate that the amount of Cu in CuSiTi that is substituted by Fe, Ni and Co increases as a function of τ at a given T_p. The Cu in CuSiTi is almost completely substituted using a T_p of 1075 °C and τ of 2 min, to give a typical composition of 3Cu–13Fe–12Ni–8Co–32Si–32Ti at.%. The quantities of Fe, Ni and Co in the ABA varied within the limits of 1–3 at.%, but no conclusive trends could be identified as a function of τ at any T_p. However, the quantities of Al and Si in the ABA significantly decreased at a T_p of 1075 °C. Before brazing, the quantities of Al and Si were measured at 4 at.% Al and 4 at.% Si. After brazing at 1075 °C, the quantity of Al was typically measured at 2.5 at.% and the amount of Si reduced to a low level, which could not be measured with confidence. These reductions in the amount of Al and Si in the ABA occurred with a significant

microstructural change involving the formation of a new phase ($Ni_{16}Si_7Ti_6$) at the ABA/Al_2O_3 interface; a detailed account of this change is given later in section 3.1.3. The amount of Si reduces to a lower amount than Al, which is likely to be a consequence of Si participating directly in the formation of phases at both the ABA/Al_2O_3 interface and ABA/Kovar® interface, while Al acts a solute in these phases.

3.1.2. Brazing 95 wt.% Al_2O_3 at 1050 °C

Increasing T_p to 1050 °C produced significant microstructural developments, particularly at the ABA/Al_2O_3 interface. Breakdown of the Si_3Ti_5 layer on the Al_2O_3 occurred much faster and to a further extent compared with brazing at a T_p of 1025 °C. BSEIs of cross-sections of 95 wt.% Al_2O_3–Kovar® joints that were held at 1050 °C for 2 to 45 min are shown in Figure 11. Brazing for 2 min produced a continuous Si_3Ti_5 layer up to ~2 μm thick on the Al_2O_3, occasionally with a number of CuSiTi particles with a typical composition of 12Cu–11Ni–10Fe–2Co–32Si–33Ti at.% alongside the Si_3Ti_5 layer. Increasing τ to 15 min broke down the Si_3Ti_5 layer significantly and produced a variation in the microstructure at the ABA/Al_2O_3 interface. No Si_3Ti_5 was observed at various positions along this interface. When Si_3Ti_5 was observed, it was either in the form of a 450 nm thick broken layer or as individual particles similar in width. CuSiTi particles were also observed at the ABA/Al_2O_3 interface, but not consistently across the interface. No evidence of Si_3Ti_5 was found after increasing τ further. Instead, individual CuSiTi particles were occasionally observed along the ABA/Al_2O_3 interface.

3.1.3. Brazing 95 wt.% Al_2O_3 at 1075 °C

BSEIs of cross-sections of 95 wt.% Al_2O_3–Kovar® joints that were held at 1075 °C for 2 to 45 min are shown in Figure 12. In a joint brazed for 2 min, the $Ni_{16}Si_7Ti_6$, Fe_2Ti and CuSiTi phases were typically observed closer to the centre of the ABA. The quantity of CuSiTi reduced to produce more Fe_2Ti, with the remaining CuSiTi typically positioned within the newly formed Fe_2Ti. $Ni_{16}Si_7Ti_6$ was consistently

observed between the Fe_2Ti and the ABA, and so $Ni_{16}Si_7Ti_6$ completely surrounded the Fe_2Ti phase. In the same joint, large single particles with a typical composition of 23Ni–18Fe–12Co–5Cu–22Si–20Ti at.% were observed on the Al_2O_3. The crystal structure of these particles was identified by electron diffraction as that of $Ni_{16}Si_7Ti_6$ (cubic, $Fm\bar{3}m$, space group 225) with the lattice parameter a = 11.7 Å. The EDS measurements are consistent with a solid solution of Fe, Co, Cu and Al in $Ni_{16}Si_7Ti_6$.

Brazing for 15 min produced a 600 nm thick $Ni_{16}Si_7Ti_6$ layer on the Al_2O_3, which was almost continuous across the entire length of the ABA/Al_2O_3 interface. Several individual $Ni_{16}Si_7Ti_6$ particles were also observed in the ABA alongside this $Ni_{16}Si_7Ti_6$ layer. No evidence of CuSiTi was found at the ABA/Al_2O_3 interface in any joint brazed at 1075 °C. At this point, the Fe_3Si layer on the Kovar® was partly broken, and so particles of Fe_3Si were found scattered throughout the ABA. The extent to which the Fe_3Si layer broke down varied across the joint, but a continuous Fe_3Si layer of at least 1.0 μm in width was typically observed on the Kovar®. In a joint brazed for 30 min, the Fe_3Si on the Kovar® was in the form of a very thin layer between ~50 nm and ~400 nm. The $Ni_{16}Si_7Ti_6$ layer on the Al_2O_3 became thicker by extending τ to 30 min, ranging from 0.5 to 2 μm. This layer was also partly broken, leaving several $Ni_{16}Si_7Ti_6$ particles alongside the $Ni_{16}Si_7Ti_6$ layer. A 3 μm thick $Ni_{16}Si_7Ti_6$ layer developed on the Al_2O_3 in a joint brazed for 45 min. In the same joint, the Fe_3Si layer on the Kovar® was typically in the form of a very thin layer. At some parts of this joint the ABA separated from the Kovar® to leave voids at the ABA/Kovar® interface.

3.2. Brazing 99.7 wt.% Al_2O_3 to Kovar®

The ABA did not bond chemically to 99.7 wt.% Al_2O_3 using a T_p of 1025 °C and τ ranging from 2 to 45 min; a BSEI of a cross-section of a joint that was brazed for 15 min is shown in Figure 13. This is because a very low level of silica-based secondary phase is present in the Al_2O_3.Notwithstanding the silicon present in the molten braze, the lack of a ready supply of silicon from the alumina has prevented the formation of a clearly identifiable Si_3Ti_5 layer at the Al_2O_3–braze interface. Close inspection of the Al_2O_3–braze interface shows some evidence of contrast consistent with the formation

of Si_3Ti_5, but it is evident that any interfacial reaction product is insignificant in comparison with that found on the 95 wt% Al_2O_3. As a consequence of the relative absence of this chemical reaction at the ABA/Al_2O_3 interface, some of the ABA flowed out of these joints.

4. Discussion

Joints containing a near-continuous 1.5–2.5 μm thick Si_3Ti_5layer on the Al_2O_3 and a continuous Fe_3Si layer on the Kovar® did not break apart on handling and could be prepared easily for microscopy. These joints were made with 95 wt.% Al_2O_3 and brazed at a T_p of 1025 °C for 0–45 min or at 1050 °C for 2 min. In a recent study [2], both alumina ceramics used in this work were brazed to themselves using a Ag–Cu–Ti-based alloy also containing a relatively small quantity of titanium, ~1.8 wt.%. This alloy began to melt at ~780 °C and then it reacted with each alumina to form Ti_3Cu_3O as the main interfacial phase. This oxide was found to be unstable at the brazing temperatures used, between 815 and 875 °C, and so it broke down, to different extents, with time at these temperatures, with the rate of this process accelerated greatly by increasing the brazing temperature. Ti_3Cu_3O was not observed in the joints made using Copper ABA® probably because it is highly unstable at temperatures equal to or greater than the liquidus temperature of Copper ABA® (i.e. the lowest brazing temperature that can be used for this ABA).

Despite the silicon in the molten braze, it is apparent from a comparison of Figures 2 and 13 that SiO_2 present in the grain boundaries of the 95 wt% Al_2O_3 is the dominant contributor to the formation of Si_3Ti_5 at the interface with 95 wt% Al_2O_3. This formation of Si_3Ti_5 on the 95 wt.% Al_2O_3 can be described by the schematic equation

$$\frac{5}{3}\,\mathrm{Ti} + \mathrm{SiO_2} \longrightarrow \frac{1}{3}\,\mathrm{Si_3Ti_5} + 2\,\mathrm{O} \qquad (1)$$

indicating that Ti diffuses to the alumina when the ABA melts to react with the SiO_2 in the alumina. Although Si_3Ti_5 can accommodate up to ~10 at.% O at 1100 °C [22], no appreciable amount of oxygen was identified in this phase. It is likely that the oxygen liberated by this reaction is dissolved into the ABA. The Al_2O_3–braze interface would seem to act as an efficient site for heterogeneous nucleation of Si_3Ti_5, so that when

there is a ready supply of silicon from the Al_2O_3 to dissolve into the molten braze, there will be a strong chemical reaction to form a near-continuous Si_3Ti_5 layer. In the absence of an additional ready supply of silicon from the Al_2O_3, the Si_3Ti_5 formed at the Al_2O_3–braze interface is insignificant, as is seen in the brazing of the 99.7 wt% Al_2O_3 to Kovar using Copper ABA.

Other Si–Ti compounds such as SiTi and Si_2Ti were not identified at the ABA/Al_2O_3 interface. These Si–Ti compounds are thermodynamically less likely to form than Si_3Ti_5 at temperatures between 1025 and 1050 °C; the Gibbs free energies of formation per mole Si at 1300 K for SiTi, Si_2Ti and Si_3Ti_5 are –129, –63 and –196 kJ mol^{-1}, respectively [23]. Si_3Ti_5 is not stable at 1025 and 1050 °C, and so it broke down chemically over time at these bonding temperatures. This decomposition of Si_3Ti_5 occurred after 15 min at 1025 °C and after 2 min at 1050 °C. The formation of CuSiTi particles at the ABA/Al_2O_3 interface near large pockets of SiO_2 in the Al_2O_3 was very noticeable at 1050 °C. A possible explanation for the formation of CuSiTi is described by the schematic reaction:

$$Ti + Cu + SiO_2 \longrightarrow CuSiTi + 2\,O \qquad (2)$$

where the oxygen liberated is likely to be dissolved into the ABA because no appreciable amount of this element was identified in the CuSiTi. No CuSiTi was observed at the ABA/Al_2O_3 interface using a $T_p \geq 1075$ °C. Furthermore, only very small amounts of CuSiTi, which appear to develop originally at the ABA/Kovar® interface and then migrated into the ABA, were observed in a joint brazed at 1075 °C for 2 min. This phase disappeared at longer bonding times to produce more Fe_2Ti in the ABA and enabled a $Ni_{16}Si_7Ti_6$ layer to form on the Al_2O_3.

It is apparent that some of the chemical elements of the CuSiTi found in the ABA, which includes significant quantities of Ni and Fe that are present by substitution of some of the Cu, diffuse to the ABA/Al_2O_3 interface after the CuSiTi decomposes. These chemical elements subsequently react with the ceramic component to form $Ni_{16}Si_7Ti_6$ on the Al_2O_3. It was not surprising that no evidence of plastic deformation of $Ni_{16}Si_7Ti_6$ was observed in the TEM, such as dislocations, because this silicide has a highly ordered crystal structure with a large unit cell, as described in [24]. By the time

a continuous $Ni_{16}Si_7Ti_6$ layer formed on the Al_2O_3, the Fe_3Si layer on the Kovar® had broken down significantly. As a consequence, all of the joints brazed using a T_p of 1075 °C broke on handling.

At the ABA/Kovar® interface, the Fe_3Si layer on the Kovar® forms very quickly and its thickness increases parabolically with time between 2 and 45 min at 1025 °C. The work of Mehrer et al. [25,26] shows that Fe diffuses much faster than Si through Fe_3Si, and so a Fe_3Si growth front may develop at the Fe_3Si/ABA interface. The $Ni_{16}Si_7Ti_6$ in the ABA appears to form on the Fe_3Si layer and then break away into the ABA. The chemical reactions leading to the formation of $Ni_{16}Si_7Ti_6$, Fe_2Ti and CuSiTi in the ABA are not clear.

Relatively few microstructural developments occurred at the ABA/Kovar® interface, compared with the ABA/Al_2O_3 interface, as a function of τ between 1025 and 1050 °C. The most significant change at the ABA/Kovar® interface was the breakdown of the Fe_3Si layer at 1075 °C with bonding times ≥15 min, which eventually resulted in separation of the ABA from the Kovar®. This microstructural development further compounds the problems of brazing at high temperatures, which include leakage of the ABA and the formation of a non-continuous brittle silicide at the ABA/Al_2O_3 interface.

The adhesion of the ABA to both the Al_2O_3 and Kovar® depends on the formation of continuous, or near-continuous, Si_3Ti_5 and Fe_3Si interfacial layers. The most appropriate brazing conditions to preserve a near-continuous Si_3Ti_5 layer on the Al_2O_3 and a continuous Fe_3Si layer on the Kovar® were found to be $\tau \leq 15$ min at a T_p of 1025 °C or ≤2 min at 1050 °C. Other conditions produced very weak bonds as a consequence of the Si_3Ti_5 and Fe_3Si layers breaking down. Further complications of brazing at a higher T_p include leakage of the ABA out of the joint and the formation of a new brittle silicide, $Ni_{16}Si_7Ti_6$, at the ABA/Al_2O_3 interface. Based on the microstructural observations made, the ranges of suitable values for T_p and τ to bond Al_2O_3 to Kovar® using Copper ABA® are quite limited, as mentioned above. It is anticipated that using this ABA to prepare large joints would not be feasible. This is

because these joints need to be held at the T_p used for several minutes to minimise any temperature gradients across the joint.

Modifying the composition of Copper ABA® by increasing the Ti content might improve the chemical interaction between the ABA and Al_2O_3 by forming a thicker and continuous Si_3Ti_5 layer (assuming that the liquidus temperature of the modified ABA is not raised to a temperature at which Si_3Ti_5 is very unstable). This could possibly increase the maximum value of τ that can be used at the liquidus temperature of the modified ABA, because it would take longer for the thicker Si_3Ti_5 layer to break down. However, larger quantities of brittle phases at the ABA/Kovar® would also form because of the strong chemical interaction between the Kovar® and the Ti in the ABA.

After an investigation of the use of Zr as an active element to braze 94 wt.% Al_2O_3 to Kovar® using 69Ag–92Cu–2Zr wt.%, Stephens et al. [27] reported that only a minor amount of Zr was consumed first in the chemical reactions between the ABA and Kovar®. As a consequence, the majority of the Zr in the ABA was available to react with the Al_2O_3 to form a ZrO_2 layer; images of the ABA/Kovar® interfaces or ABA/Al_2O_3 interfaces of the joints are not provided in report of Stephens et al. [27]. A tentative conclusion from the work of Stephens et al. [27] is that Zr is less reactive compared to Ti at the ABA/Kovar® interface. If Zr is indeed relatively less reactive with Kovar®, it might be worthwhile to investigate other Zr-containing ABAs that can be used at high temperatures in service than more commonly used Ag–Cu–Ti-based ABAs.

5. Conclusions

The ability to bond Al_2O_3 to Kovar® chemically using Copper ABA® has been investigated. The interfacial phases forming over a wide range of conditions have been identified and the effects of altering various brazing parameters, such T_p and τ, on the resultant microstructure have been determined.

It was necessary to have a small amount of silica as a secondary phase in the Al_2O_3 to bond the Al_2O_3 component to the ABA chemically. This occurred in joints made at a T_p between 1025 and 1050 °C by a reaction between Ti in the ABA and the silica to produce a layer of Si_3Ti_5 at the ABA/Al_2O_3 interface. These joints also contained a

layer of Fe_3Si on the Kovar®, along with $Ni_{16}Si_7Ti_6$, Fe_2Ti, and CuSiTi in the ABA, near the ABA/Kovar® interface, either in the form of a layered structure or a collection of individual particles. The Si_3Ti_5 layer broke down between 1025 and 1050 °C as a function of τ. In order to preserve a near-continuous Si_3Ti_5 layer on the Al_2O_3, and also a continuous Fe_3Si layer on the Kovar®, brazing conditions of $\tau \leq 15$ min at a T_p of 1025 °C or ≤2 min at 1050 °C were suitable. All joints prepared at a $T_p \geq 1050$ °C with $\tau > 2$ min broke apart on handling. This is because the Si_3Ti_5 layer on the Al_2O_3 broke down almost completely, to be replaced eventually by the brittle silicide $Ni_{16}Si_7Ti_6$ at 1075 °C, and the Fe_3Si layer on the Kovar® also broke down.

The ABA/Al_2O_3 interface is very sensitive to changes to the brazing cycle, particularly the T_p used. The degree of adhesion of the ABA to the Al_2O_3 depends on the formation of a Si_3Ti_5 interfacial layer, which requires some siliceous phase to be present at the surface of the Al_2O_3. If very high purity Al_2O_3 has to be used with Copper ABA®, the bonding surface of the Al_2O_3 should be modified to introduce a siliceous phase, so that the ABA bonds to the Al_2O_3 chemically. However, it has been shown that even using Al_2O_3 containing silica as a secondary phase, it is not straightforward to join the Al_2O_3 to Kovar® using this ABA.

Acknowledgements

We are grateful for the financial support for this study provided by AWE.

References

[1] J.A. Fernie, R.A.L. Drew, and K.M. Knowles, *Joining of engineering ceramics*, Int. Mater. Rev. 54 (2009), pp. 283–331.

[2] M. Ali, K.M. Knowles, P.M. Mallinson, and J.A. Fernie, *Microstructural evolution and characterisation of interfacial phases in Al_2O_3/Ag–Cu–Ti/Al_2O_3 braze joints*, Acta Mater. 96 (2015), pp. 143–158.

[3] M. Ali, K.M. Knowles, P.M. Mallinson, and J.A. Fernie, *Interfacial reactions between sapphire and Ag–Cu–Ti-based active braze alloys*, Acta Mater. 103 (2016), pp. 859–869.

[4] K.M. Jasim, F.A. Hashim, R.H. Yousif, R.D. Rawlings, and A.R. Boccaccini, *Actively brazed alumina to alumina joints using CuTi, CuZr and eutectic AgCuTi filler alloys*, Ceram. Int. 36 (2010), pp. 2287–2295.

[5] Y.C. Yoo, J.H. Kim, and K. Park, *Microstructural characterisation of Al_2O_3/AISI 8650 steel joint brazed with Ag-Cu-Sn-Zr*, Mater. Lett. 42 (2000), pp. 362–366.

[6] R.E. Loehman and A.P. Tomsia, *Reactions of Ti and Zr with AlN and Al_2O_3*, Acta Metall. Mater. 40 (1992), pp. S75–S83.

[7] R.E. Loehman, F.M. Hosking, B. Gauntt, and P.G. Kotula, *Reactions of Hf-Ag and Zr-Ag alloys with Al_2O_3 at elevated temperatures*, J. Mater. Sci. 40 (2005), pp. 2319–2324.

[8] M. Ali, K.M. Knowles, P.M. Mallinson, and J.A. Fernie, *Evolution of the interfacial phases in Al_2O_3–Kovar® joints brazed using a Ag–Cu–Ti-based alloy*, Philos. Mag 97 (2017), pp. 718–742.

[9] Lee D.B., Woo J.H., and Park S.W., *Oxidation behavior of Ag-Cu-Ti brazing alloys*, Mater. Sci. Eng. A. 268 (1999), pp. 202–207.

[10] Available at: http://www.morganbrazealloys.com/en-gb/resources/mechanical-physical-properties (accessed 7 October 2016).

[11] J.M. Fernandez, R. Asthana, M. Singh, and F.M. Valera, *Active metal brazing of silicon nitride ceramics using a Cu-based alloy and refractory metal interlayers*, Ceram. Int. 42 (2016), pp. 5447–5454.

[12] M. Singh, J.M. Fernandez, R. Asthana, and J.R. Rico, *Interfacial characterization of silicon nitride/silicon nitride joints brazed using a Cu-base active metal interlayers*, Ceram. Int. 38 (2012), pp. 2793–2802.

[13] M. Singh, R. Asthana, F.M. Varela, and J.M. Fernandez, *Microstructural and*

mechanical evaluation of a Cu-based active braze alloy to join silicon nitride ceramics, J. Eur. Ceram. Soc. 31 (2011), pp. 1309–1316.
[14] M. Singh, T.P. Shpargel, and R. Asthana, *Brazing of yttria-stabilized zirconia (YSZ) to stainless steel using Cu, Ag, and Ti-based brazes*, J. Mater. Sci. 43 (2008), pp. 23–32.
[15] R. Asthana, M. Singh, H.T. Lin, T. Matsunaga, and T. Ishikawa, *Joining of SiC fiber-bonded ceramics using silver, copper, nickel, palladium, and silicon-based alloy interlayers*, Int. J. Ceram. Technol. 10 (2013), pp. 801–813.
[16] Durov A.V., Kostjuk B.D., Shevchenko A.V., and Naidich Y.V., *Joining of zirconia to metal with Cu–Ga–Ti and Cu– Sn–Pb–Ti fillers*, Mater. Sci. Eng. A. 290 (2000), pp. 186–189.
[17] Durov A.V., Naidich Y.V., and Kostyuk B.D., *Investigation of interaction of metal melts and zirconia*, J. Mater. Sci. 40 (2005), pp. 2173–2178.
[18] Lin C.-C., Chen R.-B., and Shiue R.-K., *A wettability study of Cu/Sn/Ti active braze alloys on alumina*, J. Mater. Sci. 36 (2001), pp. 2145–2150.
[19] D. Tomus and H.P. Ng, *In situ lift-out dedicated techniques using FIB–SEM system for TEM specimen preparation*, Micron 44 (2013), pp. 115–119.
[20] V. Raghavan, *Fe-Ni-Si (iron-nickel-silicon)*, J. Phase Equilib. 24 (2003), pp. 269–271.
[21] V. Raghavan, *Fe-Si-Ti (iron-silicon-titanium)*, J. Phase Equilib. Diff. 30 (2009), pp. 393–396.
[22] J.I. Goldstein, S.K. Choi, F.J.J. Van Loo, G.F. Bastin, and R. Metselaar, *Solid-state reactions and phase relations in the Ti-Si-O system at 1373 K*, J. Am. Ceram. Soc. 78 (1995), pp. 313–322.
[23] I. Barin, *Thermodynamic Data of Pure Substances*, 3rd ed., VCH Verlagsgesellschaft mbH, Weinheim, 1995.
[24] A. Mateo, L. Llanes, M. Anglada, A. Redjaïmia, and G. Metauer, *Characterization of the intermetallic G-phase in an AISI 329 duplex stainless steel*, J. Mater. Sci. 32 (1997), pp. 4533–4540.
[25] H. Mehrer, M. Eggersmann, A. Gude, M. Salamon, and B. Sepiol, *Diffusion in intermetallic phases of the Fe–Al and Fe–Si systems*, Mater. Sci. Eng. A239–240 (1997), pp. 889–898.

[26] A. Gude and H. Mehrer, *Diffusion in the $D0_3$-type intermetallic phase Fe_3Si*, Philos. Mag. A 76 (1997), pp. 1–29.
[27] Stephens J.J., Vianco P.T., Hlava P.F. and Walker C.A., *Microstructure and performance of Kovar/alumina joints made with silver-copper base active metal braze alloys*, International Brazing and Soldering Conference, Albuquerque, New Mexico, USA, 2000.

Figure Captions

Figure 1. BSEIs of a cross-section of Copper ABA® captured after resting the ABA on a stainless steel support and mounting in an acrylic polymer.

Figure 2. BSEIs of cross-sections of 95 wt.% Al_2O_3/Copper ABA®/Kovar® joints that were held at 1025 °C for a) 0 min, b) 2 min, c) 15 min, d) 30 min and e) 45 min.

Figure 3. a) TEM bright field image of Si_3Ti_5 particles at the ABA/Al_2O_3 interface in a 95 wt.% Al_2O_3–Kovar® joint that was held at 1025 °C for 0 min, along with electron diffraction patterns from Si_3Ti_5 with the zone axes b) $[2\bar{1}\bar{1}0]$, c) $[4\bar{2}\bar{2}3]$ and d) $[2\bar{1}\bar{1}3]$.

Figure 4. BSEIs of a 95 wt.% Al_2O_3/Copper ABA®/Kovar® joint that was held at 1025 °C for a nominal 1 s before cooling which concentrate on a part of the joint where CuSiTi has formed next to a large quantity of silica in the Al_2O_3.

Figure 5. Electron diffraction patterns from CuSiTi found at the ABA/Al_2O_3 interface in a 95 wt.% Al_2O_3–Kovar® joint that was held at 1025 °C for 0 min, with the zone axes a) [021], b) [011] and c) [001]. $h00$ reflections where $h = 2n+1$ are present in the [021] and [011] patterns as a consequence of double diffraction.

Figure 6. a) TEM bright field image of a Fe_3Si layer at the ABA/Kovar® interface in a 95 wt.% Al_2O_3–Kovar® joint that was held at 1025 °C for 0 min, along with electron diffraction patterns from Fe_3Si with the zone axes a) [010], b) [011] and c) [111].

Figure 7. a) TEM bright field image of $Ni_{16}Si_7Ti_6$ found near the ABA/Kovar® interface in a 95 wt.% Al_2O_3–Kovar® joint that was held at 1025 °C for 0 min, along with electron diffraction patterns from $Ni_{16}Si_7Ti_6$ with the zone axes a) [111], b) [112] and c) [001].

Figure 8. Electron diffraction patterns from Fe_2Ti found near the ABA/Kovar® interface in a 95 wt.% Al_2O_3–Kovar® joint that was held at 1025 °C for 0 min, with the zone axes a) $[0001]$, b) $[11\bar{2}6]$ and c) $[11\bar{2}3]$.

Figure 9. a) TEM bright field images of a CuSiTi particle found near the ABA/Kovar® interface in a 95 wt.% Al_2O_3–Kovar® joint that was held at 1025 °C for 0 min; some of the dislocations in this particle are pinned to Cu inclusions. Electron diffraction patterns from CuSiTi are shown with the zone axes b) [010], c) [120] and d) [110].

Figure 10. Thicknesses of the Fe_3Si layers formed in 95 wt.% Al_2O_3/Copper ABA®/Kovar® joints as a function of $\tau^{\frac{1}{2}}$ for the different T_p used.

Figure 11. BSEIs of cross-sections of 95 wt.% Al_2O_3/Copper ABA®/Kovar® joints that were held at 1050 °C for a) 2 min, b) 15 min, c) 30 min and d) 45 min.

Figure 12. BSEIs of cross-sections of 95 wt.% Al_2O_3/Copper ABA®/Kovar® joints that were held at 1075 °C for a) 2 min, b) 15 min, c) 30 min and d) 45 min.

Figure 13. BSEIs of a cross-section of a 99.7 wt.% Al_2O_3/Copper ABA®/Kovar® joint that was held at 1025 °C for 15 min.

Table 1. Chemical composition of the 95 wt.% and 99.7 wt.% Al_2O_3 components used in wt.%. Average values from 30 electron microprobe measurements with errors of ± one standard deviation reported. *The quantities of these elements were below or approximately equal to the detection limit.

Al_2O_3 purity/ wt.% Al_2O_3	**Al**	**O**	**Si**	**Na**	**Mg**	**Ca**	**Fe**	**Zr**
99.7	55.4 ±1.3	44.0 ±1.5	0.2 ±0.1	0.0*	0.3 ±0.1	0.0*	0.0*	0.0*
95	52.2 ±1.9	43.5 ±1.6	2.5 ±0.4	0.3 ±0.1	0.4 ±0.2	0.6 ±0.2	0.2 ±0.1	0.3 ±0.1

Table 2. T_p and τ used to braze 95 and 99.7 wt.% Al_2O_3. *Joints made with 95 wt.% Al_2O_3 using these conditions and all joints made with 99.7 wt.% Al_2O_3 were mounted in clear resin before cutting out cross-sections to avoid detaching the Al_2O_3 from the ABA.

	1025 °C	**1050 °C**	**1075 °C**	**1100 °C**
0 min	95 wt.%	–	–	–
2 min	95 and 99.7 wt.%	95 wt.%	*95 wt.%	*95 wt.%
15 min	95 and 99.7 wt.%	*95 wt.%	*95 wt.%	–
30 min	95 and 99.7 wt.%	*95 wt.%	*95 wt.%	–
45 min	95 and 99.7 wt.%	*95 wt.%	*95 wt.%	–

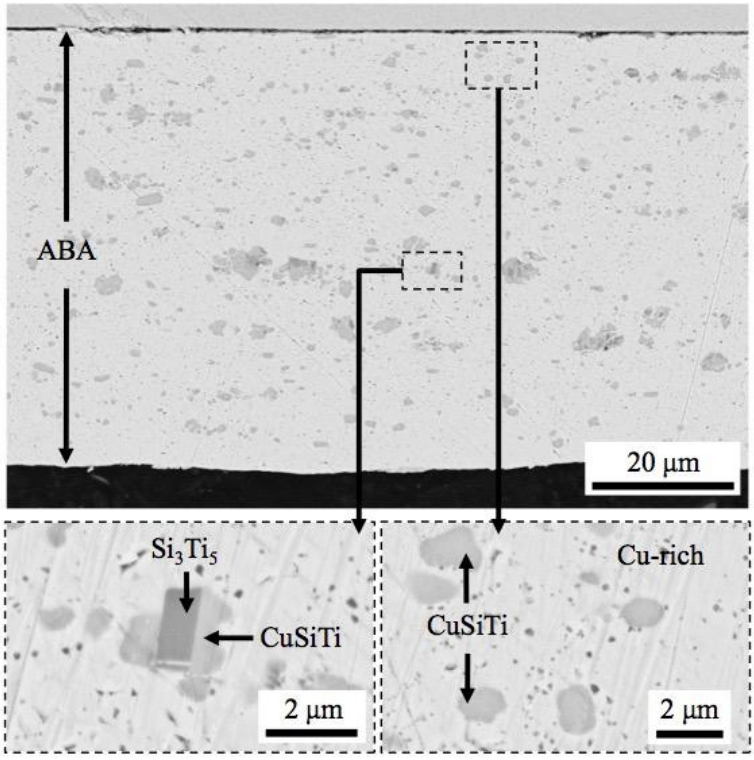

Figure 1. BSEIs of a cross-section of Copper ABA® captured after resting the ABA on a stainless steel support and mounting in an acrylic polymer.

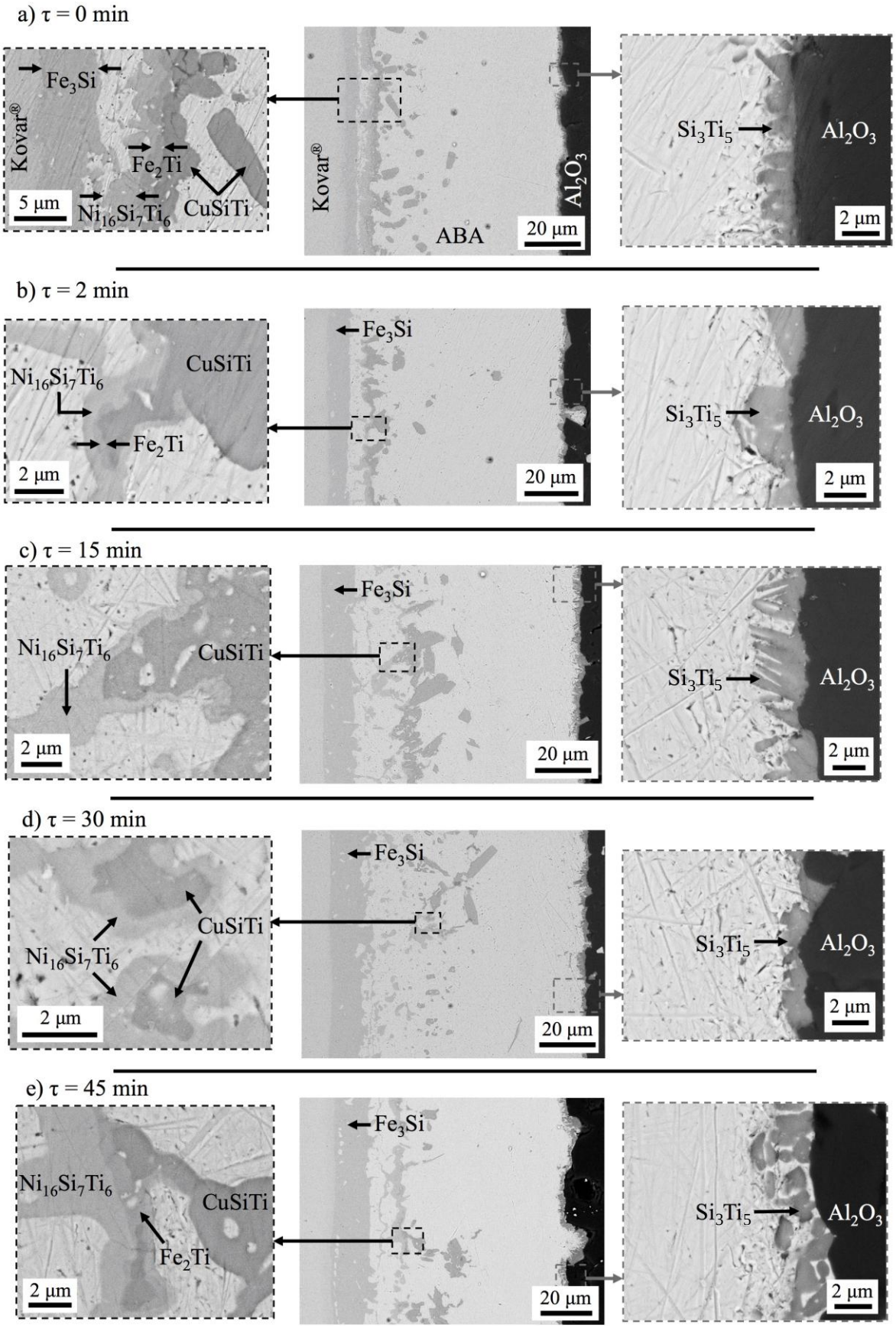

Figure 2. BSEIs of cross-sections of 95 wt.% Al_2O_3/Copper ABA®/Kovar® joints that were held at 1025 °C for a) 0 min, b) 2 min, c) 15 min, d) 30 min and e) 45 min.

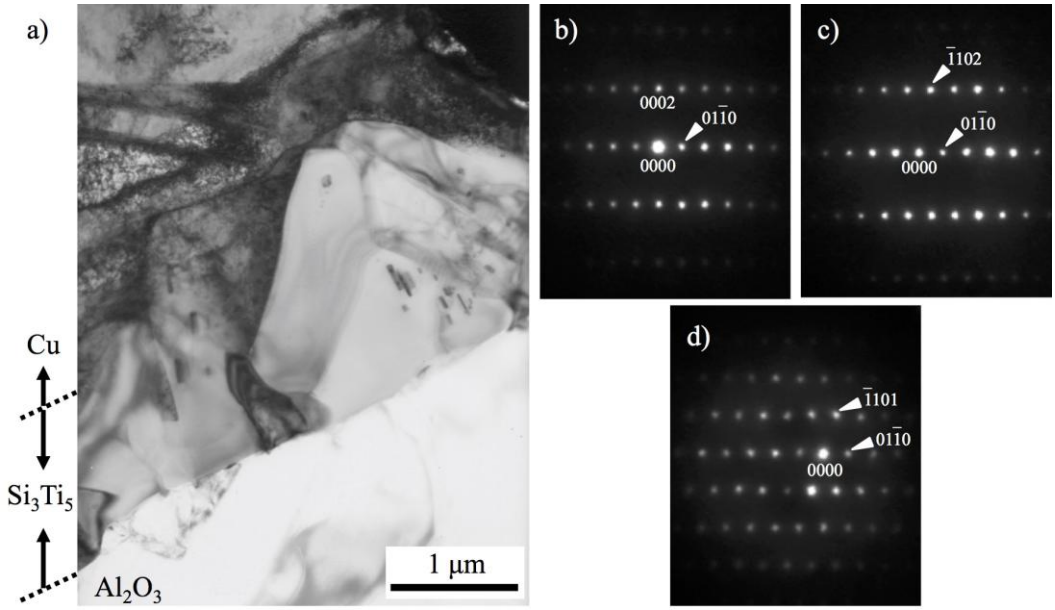

Figure 3. a) TEM bright field image of Si_3Ti_5 particles at the ABA/Al_2O_3 interface in a 95 wt.% Al_2O_3–Kovar® joint that was held at 1025 °C for 0 min, along with electron diffraction patterns from Si_3Ti_5 with the zone axes b) $[2\bar{1}\bar{1}0]$, c) $[4\bar{2}\bar{2}3]$ and d) $[2\bar{1}\bar{1}3]$.

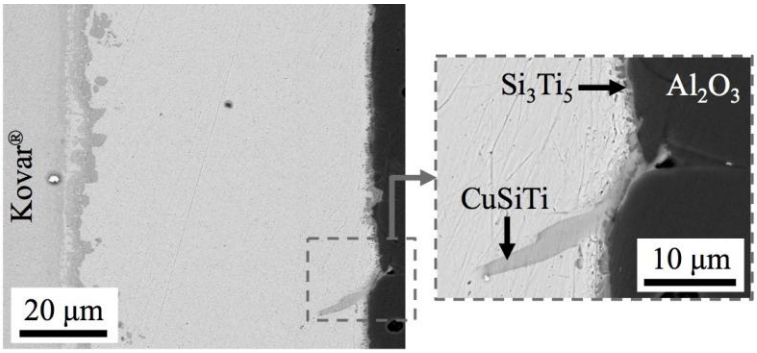

Figure 4. BSEIs of a 95 wt.% Al_2O_3/Copper ABA®/Kovar® joint that was held at 1025 °C for a nominal 1 s before cooling which concentrate on a part of the joint where CuSiTi has formed next to a large quantity of silica in the Al_2O_3.

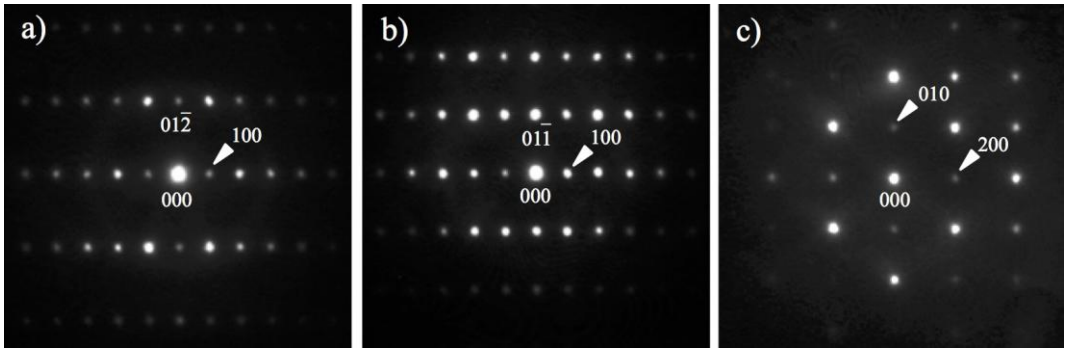

Figure 5. Electron diffraction patterns from CuSiTi found at the ABA/Al_2O_3 interface in a 95 wt.% Al_2O_3–Kovar® joint that was held at 1025 °C for 0 min, with the zone axes a) [021], b) [011] and c) [001]. *h*00 reflections where $h = 2n+1$ are present in the [021] and [011] patterns as a consequence of double diffraction.

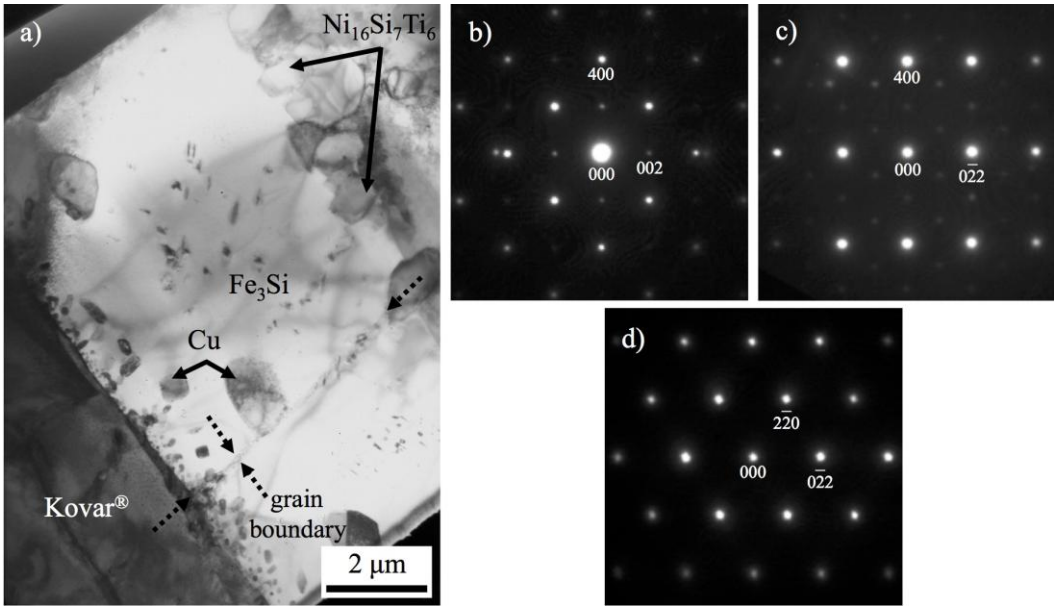

Figure 6. a) TEM bright field image of a Fe_3Si layer at the ABA/Kovar® interface in a 95 wt.% Al_2O_3–Kovar® joint that was held at 1025 °C for 0 min, along with electron diffraction patterns from Fe_3Si with the zone axes a) [010], b) [011] and c) [111].

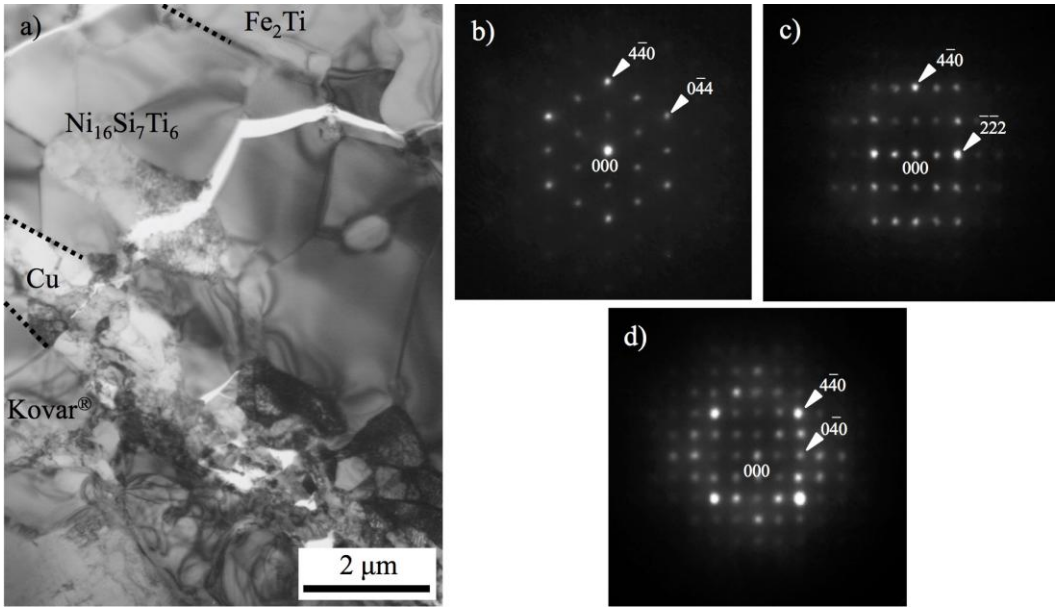

Figure 7. a) TEM bright field image of a $Ni_{16}Si_7Ti_6$ layer found near the ABA/Kovar® interface in a 95 wt.% Al_2O_3–Kovar® joint that was held at 1025 °C for 0 min, along with electron diffraction patterns from $Ni_{16}Si_7Ti_6$ with the zone axes a) [111], b) [112] and c) [001].

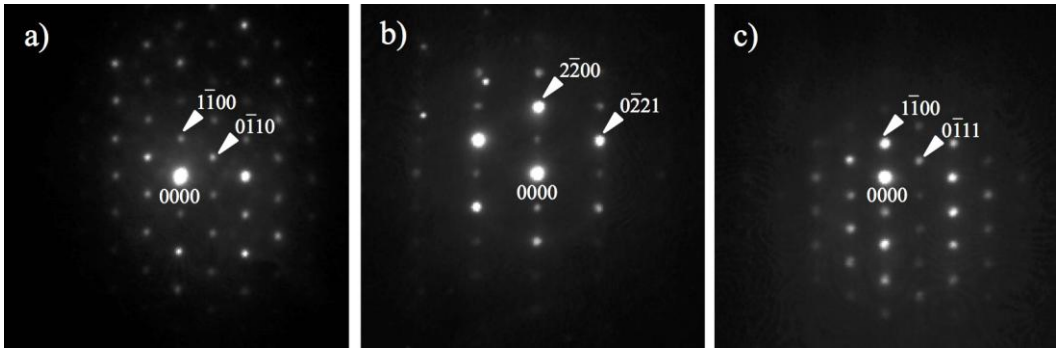

Figure 8. Electron diffraction patterns from Fe_2Ti found near the ABA/Kovar® interface in a 95 wt.% Al_2O_3–Kovar® joint that was held at 1025 °C for 0 min, with the zone axes a) [0001], b) [11$\bar{2}$6] and c) [11$\bar{2}$3].

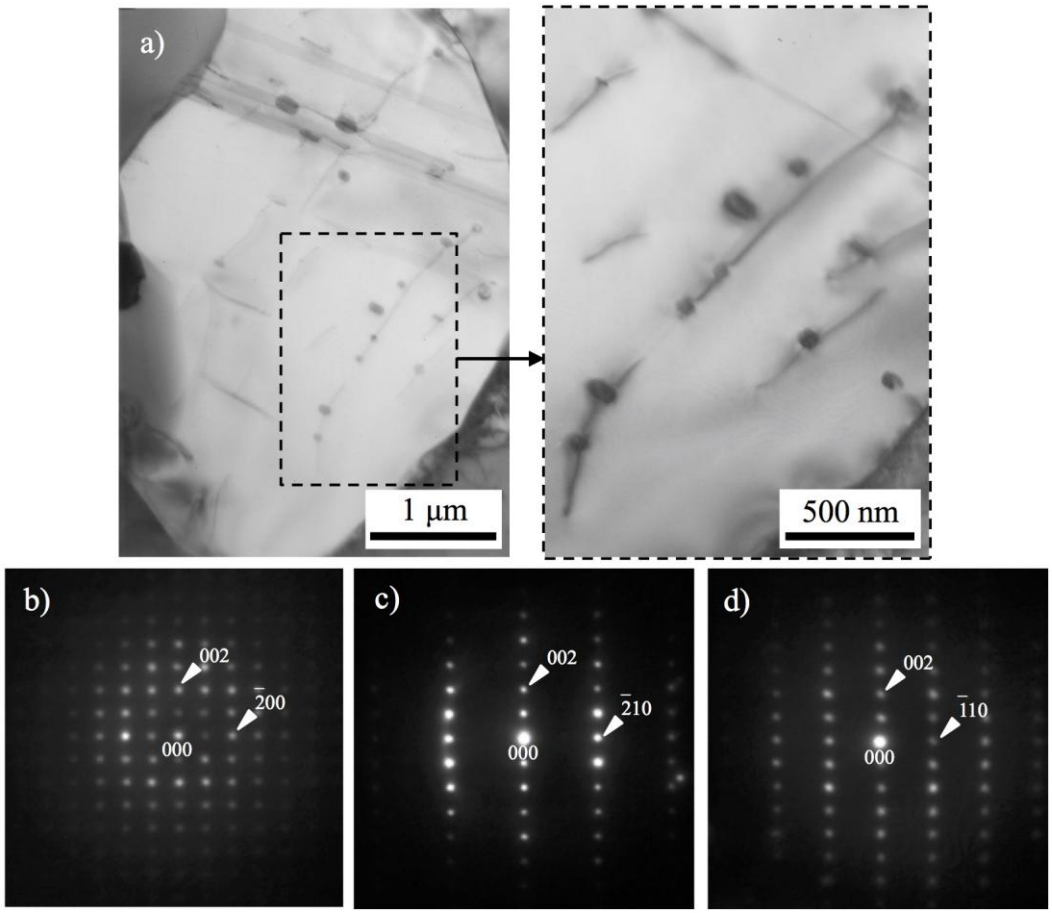

Figure 9. a) TEM bright field images of a CuSiTi particle found near the ABA/Kovar® interface in a 95 wt.% Al_2O_3–Kovar® joint that was held at 1025 °C for 0 min; some of the dislocations in this particle are pinned to Cu inclusions. Electron diffraction patterns from CuSiTi are shown with the zone axes b) [010], c) [120] and d) [110].

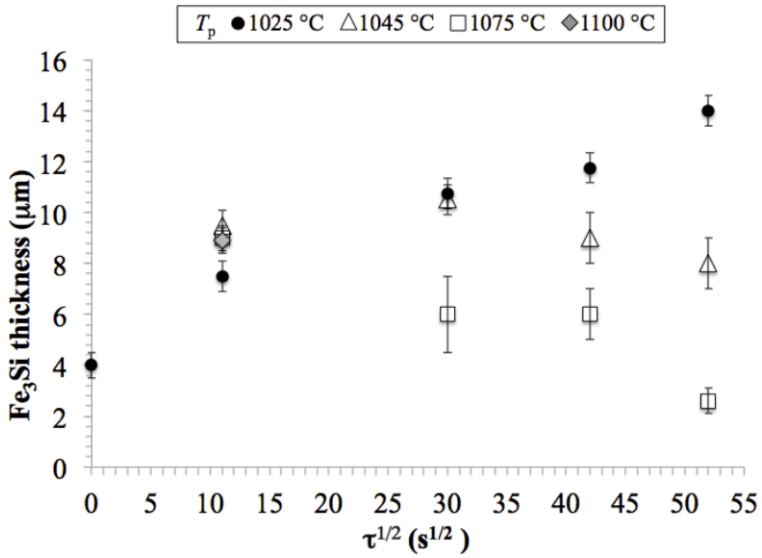

Figure 10. Thicknesses of the Fe_3Si layers formed in 95 wt.% Al_2O_3/Copper ABA®/Kovar® joints as a function of $\tau^{\frac{1}{2}}$ for the different T_p used.

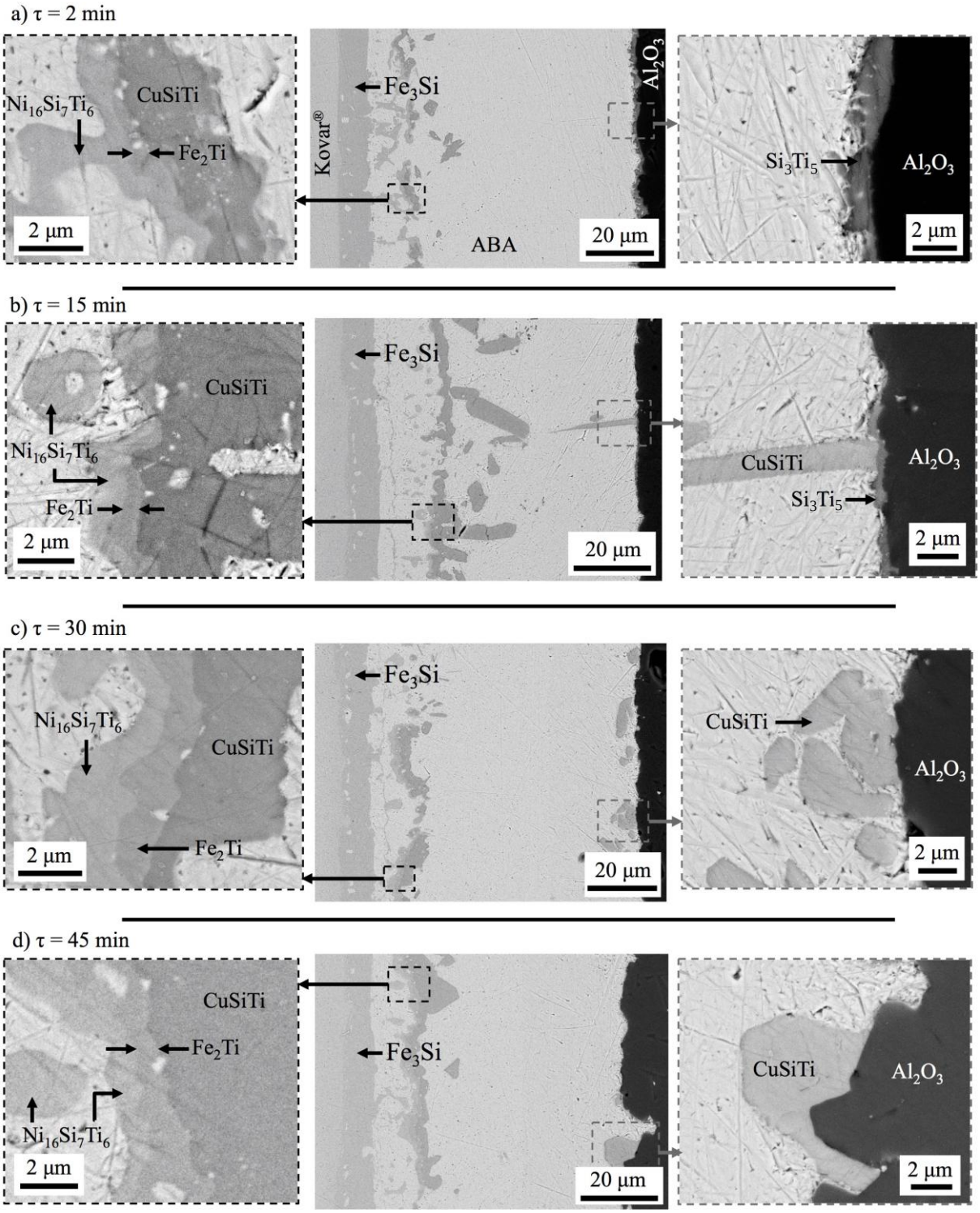

Figure 11. BSEIs of cross-sections of 95 wt.% Al_2O_3/Copper ABA®/Kovar® joints that were held at 1050 °C for a) 2 min, b) 15 min, c) 30 min and d) 45 min.

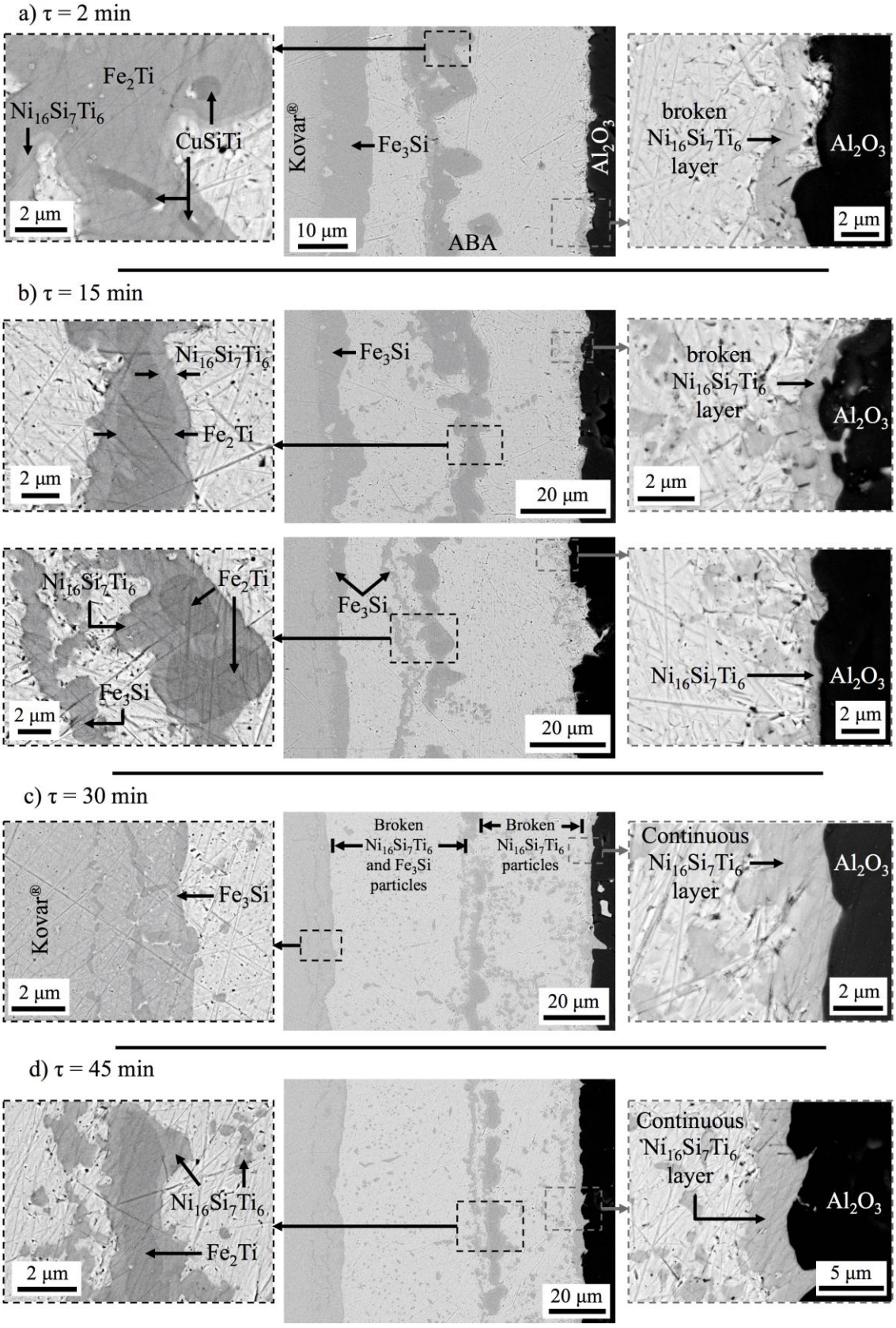

Figure 12. BSEIs of cross-sections of 95 wt.% Al_2O_3/Copper ABA®/Kovar® joints that were held at 1075 °C for a) 2 min, b) 15 min, c) 30 min and d) 45 min.

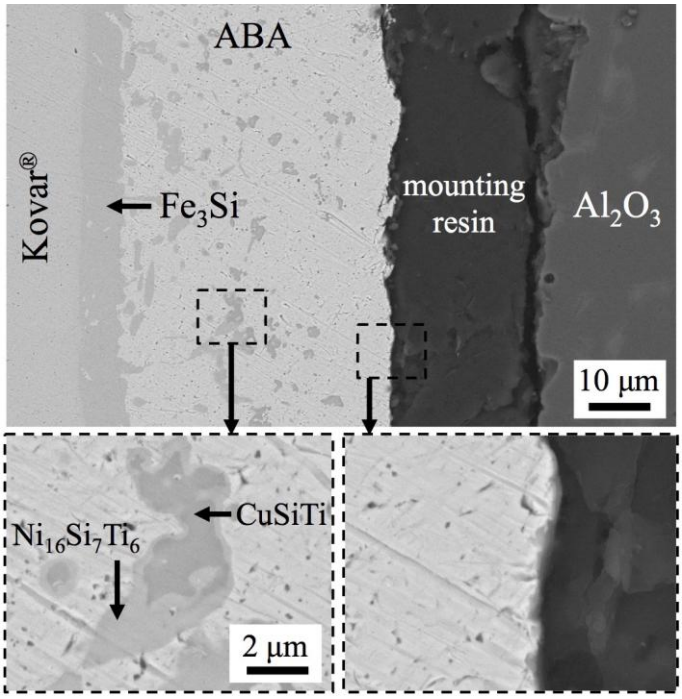

Figure 13. BSEIs of a cross-section of a 99.7 wt.% Al_2O_3/Copper ABA®/Kovar® joint that was held at 1025 °C for 15 min.